TITLE*

Brage A. Trefjord
Department of Physics, University of Oslo, Norway
(Dated: April 10, 2024)

Abstract

Keywords: Keywords

I. INTRODUCTION

Husk å referere til nettsiden til Winther for likninger. [1]

II. MILESTONE I
BACKGROUND COSMOLOGY

In order to compute the CMB power spectrum there are several different values that we will need, and in this milestone we have computed some of the most important background parameters needed to deal with the structure and evolution of the universe. This includes the different measures of time, namely cosmic time, conformal time and redshift; the different measures of distance, namely co-moving distance, angular diameter distance and luminosity distance; the Hubble parameter and the conformal Hubble parameter; and the densities of the different consituents that make up the universe, namely photons, neutrinos, baryons, dark matter and dark energy. Lastly, we also tested the theoretical predictions by comparing to observational data from supernovas [2].

A. Theory

1. Time variables

Any value that is monotonically increasing (or decreasing) with time can be used as a measure of the time that has passed since the big bang. Which time variable that is most convenient to work with might vary between different applications. One such time variable is the scalefactor a of the universe. a is defined to be relative size of the universe compared to today. In other words, $a_0 = a(\text{today}) = 1$. We will often have use of the logarithm of the scalefactor, since we want to explore values that vary a lot over small changes in the scalefactor, and we define this as its own time variable, namely

$$x = \log a. \tag{1}$$

In addition, we will need the conformal time η, defined by

$$\frac{d\eta}{dt} = \frac{c}{a}, \tag{2}$$

also called the horizon. η is the distance that light may have travelled since the big bang ($t = 0$). We can rewrite Eq. 2 by substituting $t \to x$. We then get

$$\frac{d\eta}{dx} = \frac{c}{\mathcal{H}}, \tag{3}$$

where $\mathcal{H} = aH$ is the conformal Hubble parameter, where $H = \frac{\dot{a}}{a}$ is the Hubble parameter. Note here that the dot denotes a derivative with respect to conformal time, i.e., $\dot{} = \frac{d}{d\eta}$.

The cosmic time t is the time experienced by an observer with no velocity, away from any gravitational field, and is given by

$$\frac{dt}{dx} = \frac{1}{H}. \tag{4}$$

The redshift z, defined by

$$1 + z = \frac{1}{a}, \tag{5}$$

is a measure of how much light will have redshifted over time, and is also used as a time variable.

The co-moving distance is

$$\chi(a) = \eta_0 - \eta(a), \tag{6}$$

where η_0 denotes the conformal time today. The co-moving distance is the distance between two points at the present time (i.e., without taking the expansion of the universe into account), namely the distance between the horizon η_0 today, and the horizon $\eta(a)$ at some scalefactor a.

We also have the angular diameter distance

$$d_A = ar, \tag{7}$$

where

$$r = \begin{cases} \chi \cdot \dfrac{\sin\left(\sqrt{|\Omega_{k0}|}H_0\chi/c\right)}{\left(\sqrt{|\Omega_{k0}|}H_0\chi/c\right)} & \Omega_{k0} < 0 \\ \chi & \Omega_{k0} = 0 \\ \chi \cdot \dfrac{\sinh\left(\sqrt{|\Omega_{k0}|}H_0\chi/c\right)}{\left(\sqrt{|\Omega_{k0}|}H_0\chi/c\right)} & \Omega_{k0} > 0 \end{cases} \tag{8}$$

which describes the expected distance to an object of known size based on the measured angle it spans. Lastly, we have the luminosity distance

$$d_L = \frac{r}{a} = \frac{d_A}{a^2}, \qquad (9)$$

which gives the expected distance to an object of known luminosity, based on the flux measured on earth. Both the angular diameter distance and the luminosity distance are based on euclidean measures of distance.

2. The geometry of the universe

We assume the early universe to be homogeneous and isotropic, and for such a universe we can use the Friedmann-Lemaître-Robertson-Walker (FLRW) metric, which is defined as

$$ds^2 = -c^2 dt^2 + a^2(t)(dx^2 + dy^2 + dz^2), \qquad (10)$$

where ds is the line element in spacetime and t and $\vec{x} = (x, y, z)$ are the spacetime components.

The Einstein equation is given by

$$G_{\mu\nu} = 8\pi G T_{\mu\nu}, \qquad (11)$$

where $G_{\mu\nu}$ is the Einstein tensor, G is Newton's gravitational constant, and $T_{\mu\nu}$ is the energy-momentum tensor. The Einstein equation relates the geometry of the universe (given by $G_{\mu\nu}$) to the distribution of energy and momentum (given by $T_{\mu\nu}$). The Einstein tensor is given by

$$G_{\mu\nu} = R_{\mu\nu} - \frac{1}{2}R g_{\mu\nu}, \qquad (12)$$

where $R_{\mu\nu}$ is the Ricci tensor, and $R = R^\mu_\mu = g^{\mu\nu}R_{\mu\nu}$ is the Ricci scalar. The Ricci tensor is in turn given by

$$R_{\mu\nu} = \Gamma^\alpha_{\mu\nu,\alpha} - \Gamma^\alpha_{\mu\alpha,\nu} + \Gamma^\alpha_{\mu\nu}\Gamma^\beta_{\alpha\beta} - \Gamma^\beta_{\mu\alpha}\Gamma^\alpha_{\beta\nu},$$

where $\Gamma^\mu_{\alpha\beta} = \frac{g^{\mu\delta}}{2}(g_{\delta\beta,\alpha} + g_{\alpha\delta,\beta} - g_{\alpha\beta,\delta})$ are the Christoffel symbols, and a comma in the indices denotes a derivative with respect to some spacetime coordinate, i.e., $\Gamma^\alpha_{\mu\nu,\beta} = \frac{\partial}{\partial x^\beta}\Gamma^\alpha_{\mu\nu}$. From expanding $G_{\mu\nu}$ it becomes clear that it is just made up of the metric tensor (although quite a few of it), which shows how Eq. 11 is related to the geometry of the universe.

3. The constituents of the universe

We assume that every constituent in the universe behave like perfect fluids. The energy-momentum tensor for a perfect fluid is

$$T_{\mu\nu} = (\rho + p)u_\mu u_\nu + p g_{\mu\nu}, \qquad (13)$$

where ρ is the energy density of the fluid, p is the pressure, u_μ is the 4-velocity of the fluid, and $g_{\mu\nu}$ is the metric tensor, which in the FRLW metric is given by $g_{00} = -1$, $g_{ij} = a^2(t)\delta_{ij}$ and any other component is zero.

If we insert the FLRW metric tensor $g_{\mu\nu}$ and the energy-momentum tensor $T_{\mu\nu}$ into Eq. 11, we get the Friedmann equation for the Hubble parameter $H = \frac{\dot{a}}{a}$, given by Eq. 14a. From this eqation, we can compute the conformal Hubble parameter $\mathcal{H} = aH$, and its derivatives with respect to x. The Hubble parameter H, the conformal Hubble parameter $\mathcal{H}$ and its derivatives $\frac{d\mathcal{H}}{dx}$ and $\frac{d^2\mathcal{H}}{dx^2}$ are given by

$$H = H_0\sqrt{(\Omega_{b0} + \Omega_{\mathrm{CDM0}})e^{-3x} + (\Omega_{\gamma 0} + \Omega_{\nu 0})e^{-4x} + \Omega_{k0}e^{-2x} + \Omega_{\Lambda 0}}, \qquad (14a)$$

$$\mathcal{H} = e^x H, \qquad (14b)$$

$$\frac{d\mathcal{H}}{dx} = \frac{H_0^2}{\mathcal{H}}\left[\Omega_{\Lambda 0}e^{2x} - (\Omega_{\gamma 0} + \Omega_{\nu 0})e^{-2x} - \frac{1}{2}(\Omega_{b0} + \Omega_{\mathrm{CDM0}})e^{-x}\right], \qquad (14c)$$

$$\frac{d^2\mathcal{H}}{dx^2} = \frac{H_0^2}{\mathcal{H}}\left[2\Omega_{\Lambda 0}e^{2x} + 2(\Omega_{\gamma 0} + \Omega_{\nu 0})e^{-2x} + \frac{1}{2}(\Omega_{b0} + \Omega_{\mathrm{CDM0}})e^{-x}\right] - \frac{1}{\mathcal{H}}\left(\frac{d\mathcal{H}}{dx}\right)^2, \qquad (14d)$$

where $H = \frac{\dot{a}}{a}$ is the Hubble parameter (the dot refers to derivative with respect to conformal time $\frac{d}{d\eta}$), $\Omega_i = \frac{\rho_i}{\rho_c}$ ($\rho_c = \frac{3H^2}{8\pi G}$ is the critical density) are the density parameters for the different constituents and a subscript 0 refers to the value today. The possible values of i are b (baryons), CDM (cold dark matter), γ (photons), ν (neutrinos), k (curvature) and Λ (dark energy). The density parameters $\Omega_{\gamma 0}$ and $\Omega_{\nu 0}$ can be computed from the ob-

served CMB temperature. We have

$$\Omega_{\gamma 0} = 2 \cdot \frac{\pi^2}{30}\frac{(k_b T_{\mathrm{CMB0}})^4}{\hbar^3 c^5} \cdot \frac{8\pi G}{3H_0^2}, \qquad (15a)$$

$$\Omega_{\nu 0} = N_{\mathrm{eff}} \cdot \frac{7}{8} \cdot \left(\frac{4}{11}\right)^{4/3}\Omega_{\gamma 0}, \qquad (15b)$$

where k_b is the Boltzmann's constant, T_{CMB0} is the CMB temperature today and N_{eff} is the effective number of

massless neutrinos.

From Einstein's equations we can also derive the following equation,

$$\frac{d\rho}{dt} + 3H(\rho + p) = 0. \tag{16}$$

Eqs. 14a and 16 are referred to as the Friedmann equations.

If we define the equation of state $\omega = \frac{P}{\rho}$, we can use Eq. 16 to find how the density parameters evolve as functions of the scalefactor a. We find the following

$$\Omega_k(a) = \frac{\Omega_{k0}}{a^2 H(a)^2 / H_0^2} \tag{17a}$$

$$\Omega_{\text{CDM}}(a) = \frac{\Omega_{\text{CDM0}}}{a^3 H(a)^2 / H_0^2} \tag{17b}$$

$$\Omega_b(a) = \frac{\Omega_{b0}}{a^3 H(a)^2 / H_0^2} \tag{17c}$$

$$\Omega_\gamma(a) = \frac{\Omega_{\gamma 0}}{a^4 H(a)^2 / H_0^2} \tag{17d}$$

$$\Omega_\nu(a) = \frac{\Omega_{\nu 0}}{a^4 H(a)^2 / H_0^2} \tag{17e}$$

$$\Omega_\Lambda(a) = \frac{\Omega_{\Lambda 0}}{H(a)^2 / H_0^2}. \tag{17f}$$

4. Analytic expressions in certain regimes

It is important to be able to test the results from our numerical computations, and one way of doing this is to compute analytical expressions in certain regimes that we can compare the numerical results with. Here, we have found some analytical expressions for the radiation dominated era and the dark energy dominated era. We have also included an expression that relates the acceleration of the universe to the conformal Hubble parameter.

a. *Radiation dominated era* In very early times, the universe is thought to be radiation dominated, i.e., it consisted mainly of photons and neutrinos. In this regime, one finds that the conformal Hubble parameter $\mathcal{H}$, and its first and second order derivative with respect to x, are given by

$$\mathcal{H}_R = H_0 e^{-x} \tag{18a}$$

$$\frac{1}{\mathcal{H}_R} \frac{d\mathcal{H}_R}{dx} = -1 \tag{18b}$$

$$\frac{1}{\mathcal{H}_R} \frac{d^2\mathcal{H}_R}{dx^2} = 1. \tag{18c}$$

The conformal time η in the radiation dominated regime is found to be

$$\eta_R(x) = \frac{c}{H_0} e^x, \tag{19}$$

and putting Eq. 18a and 19 together we find that

$$\frac{\eta_R \mathcal{H}_R}{c} = 1, . \tag{20}$$

b. *Matter dominated era* As with the radiation dominated era, we can find some analytical expressions for a matter dominated universe, i.e., when the universe mainly consisted of baryons and dark matter. In this regime, the conformal Hubble parameter and its derivatives are

$$\mathcal{H}_M = H_0 e^{-\frac{1}{2}x} \tag{21a}$$

$$\frac{1}{\mathcal{H}_M} \frac{d\mathcal{H}_M}{dx} = -\frac{1}{2} \tag{21b}$$

$$\frac{1}{\mathcal{H}_M} \frac{d^2\mathcal{H}_M}{dx^2} = \frac{1}{4}. \tag{21c}$$

c. *Dark energy dominated era* We can also find some analytical expressions for a dark energy dominated universe. When the universe mainly consists of dark energy, the conformal Hubble parameter $\mathcal{H}$ and its derivatives with respect to x are

$$\mathcal{H}_{\text{DE}} = H_0 e^x \tag{22a}$$

$$\frac{1}{\mathcal{H}_{\text{DE}}} \frac{d\mathcal{H}_{\text{DE}}}{dx} = 1 \tag{22b}$$

$$\frac{1}{\mathcal{H}_{\text{DE}}} \frac{d^2\mathcal{H}_{\text{DE}}}{dx^2} = 1. \tag{22c}$$

d. *Acceleration of the universe* At a certain point, the expansion of the universe begins to accelerate. a is the scalefactor of the universe, and $\ddot{a}$ is the acceleration of the scalefactor with respect to conformal time η, so the expansion of the universe accelerates if $\ddot{a} > 0$. We can relate this acceleration to the conformal Hubble parameter $\mathcal{H}$ by

$$\ddot{a} = \frac{d\dot{a}}{d\eta} = \frac{d\dot{a}}{dx}\frac{dx}{d\eta} = \frac{d\mathcal{H}}{dx}\frac{1}{\frac{d\eta}{dx}} = \frac{\mathcal{H}}{c}\frac{d\mathcal{H}}{dx}.$$

$\mathcal{H}$ is always positive, thus $\ddot{a} > 0$ if and only if $\frac{d\mathcal{H}}{dx} > 0$, and so the universe is accelerating when $\frac{d\mathcal{H}}{dx} > 0$.

B. Implementation details

In the numerical calculations we have used the parameters that were found as best fits in the Planck paper [3]. These values are

$$h = 0.67,$$
$$T_{\text{CMB0}} = 2.7255\,K,$$
$$N_{\text{eff}} = 3.046,$$
$$\Omega_{\text{b0}} = 0.05,$$
$$\Omega_{\text{CDM0}} = 0.267,$$
$$\Omega_{k0} = 0,$$
$$\Omega_{\Lambda 0} = 1 - (\Omega_{k0} + \Omega_{b0} + \Omega_{\text{CDM0}} + \Omega_{\gamma 0} + \Omega_{\nu 0}),$$

where h is defined such that $H_0 = 100\,h\,\text{km}/(\text{s\,Mpc})$. From these values we also computed Ω_γ and Ω_ν using Eq. 15.

Using these values we computed the Hubble H, the conformal Hubble parameter $\mathcal{H}$, and the first and second derivatives of $\mathcal{H}$ for different values of x using Eqs. 14. We found the co-moving distance χ using Eq. 6, the angular diameter distance d_A using Eq. 7 and the luminosity distance d_L using Eq. 9

In order to compute the conformal time η and the cosmic time t we used a Runge-Kutta 4 ODE solver to solve Eq.3 and 4, and created cubic splines for both η and t.

Lastly, we looked at observational data from supernovas, taken from [2]. This dataset consisted of the luminosity distance of the supernovas for different redshifts (together with their errors). We used a Markoc chain Monte Carlo (MCMC), namely the Metropolis algorithm [4], to sample from this dataset. Each sample of the MCMC algorithm gave us a χ^2-, h-, Ω_M- and Ω_K-value, where χ^2 is the chi-squared function and $\Omega_M = \Omega_b + \Omega_{\mathrm{CDM}}$ is the matter density parameter. From Ω_M and Ω_K we found $\Omega_\Lambda = 1 - \Omega_M - \Omega_K$ (here we assume that there is no radiation at the relevant redshifts). We found which samples were within the 1σ and 2σ confidence regions of the samples (σ referring to the standard deviation), by comparing the χ^2 values to the 1σ and 2σ constraints given by [5]. We do the fitting with three free parameters, thus the 1σ confidence region is given by the samples where $\chi^2 - \chi^2_{\min} < 3.53$, and the 2σ confidence region is given by the samples where $\chi^2 - \chi^2_{\min} < 8.02$. Here $\chi^2_{\min}$ denotes the smallest χ^2-value across the samples.

C. Results

In Fig. 1 we have plotted the first and second derivatives of the conformal Hubble factor $\mathcal{H}$. We see that $\frac{1}{\mathcal{H}}\frac{d\mathcal{H}}{dx} \to -1$, and $\frac{1}{\mathcal{H}}\frac{d^2\mathcal{H}}{dx^2} \to 1$, as $a \to 0$, which corresponds with Eqs. 18 for a radiation dominated universe. This is exactly what we expect for $a \to 0$, since the early universe was radiation dominated. We also see that both the first and second derivatives converge to 1 as a becomes large. This corresponds well with Eqs. 22 for a dark energy dominated universe, which is what we expect the universe to be as time evolves. The point where $\frac{1}{\mathcal{H}}\frac{d\mathcal{H}}{dx} = 0$ shows the time where the expansion of the universe starts to accelerate.

In Fig. 2 we have plotted the product $\frac{\eta\mathcal{H}}{c}$ as a function of the scalefactor a. We see that $\frac{\eta\mathcal{H}}{c} \to 1$ as $a \to 0$, which corresponds well with Eq. 20 for the radiation dominated early universe.

In Fig. 3 you can see how the conformal Hubble factor $\mathcal{H}$ evolves with the scalefactor a. The curve decreases exponentially to start with (straight line in the log-log plot), which corresponds well with Eq. 18a for a radiation dominated universe. After a while, the slope in Fig. 3 changes, and at $a = 0.62$ (shown with a vertical dotted line), $\mathcal{H}$ begins to increase exponentially. The point where $\mathcal{H}$ starts to increase exponentially corresponds to the universe beginning to accelerate.
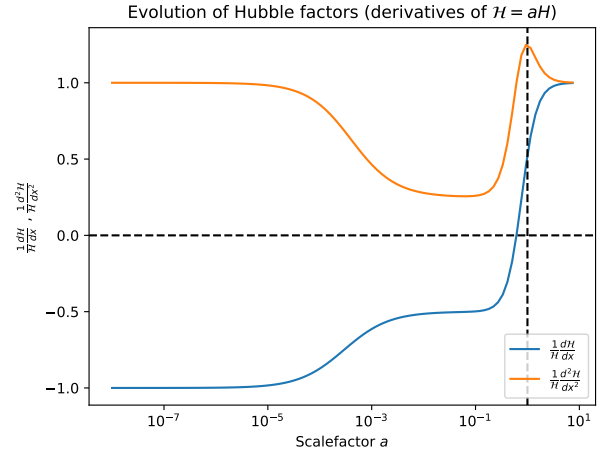

FIG. 1. First and second derivatives of the conformal Hubble factor $\mathcal{H}$ as functions of the scalefactor a. The vertical line at $a = 1$ shows the present day. The horizontal line at $y = 0$ shows where the derivative $\frac{1}{\mathcal{H}}\frac{d\mathcal{H}}{dx} = 0$.
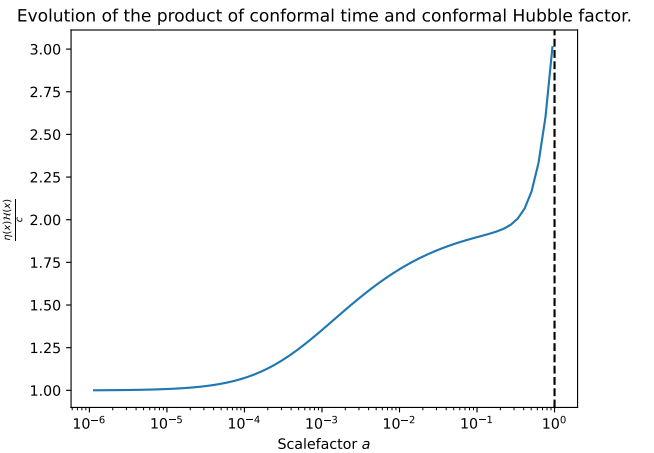

FIG. 2. $\frac{\eta\mathcal{H}}{c}$ as a function of the scalefactor a. The vertical line at $a = 1$ shows the present day.

In Fig. 4 we have plotted the cosmic time t as a function of the scalefactor a. From this plot we can clearly see that the universe expands with time, which is a good confirmation that our use of the scalefactor as a time variable is sensible. At $a = 0.62$ (represented by the vertical dotted line) the curve starts to bend downwards. This corresponds to the point where the expansion of the universe begins to accelerate.

The evolution of the conformal time η as a function of the scalefactor a is shown in Fig. 5. The conformal time increases with the scalefactor, which fits well with the conformal time corresponding to the radius of the observable universe. We can also see that the conformal time increases exponentially in the beginning (linearly in the log-log plot), in accordance with Eq.19 for a radiation
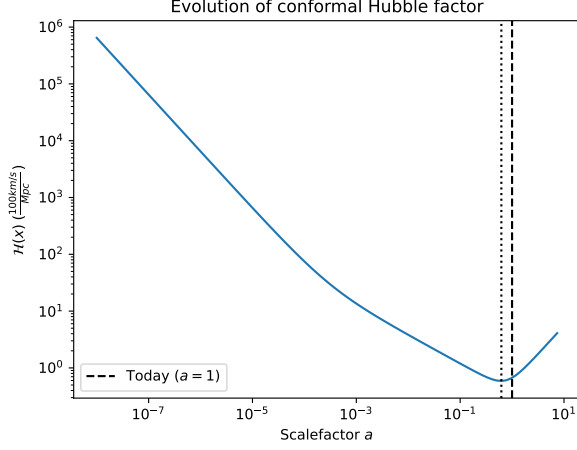
FIG. 3. The conformal Hubble factor $\mathcal{H}$ as a function of the scalefactor a. The vertical dotted line at $a = 0.62$ corresponds to the the point where the universe begins to accelerate, and the vertical dashed line at $a = 1$ shows the present day.
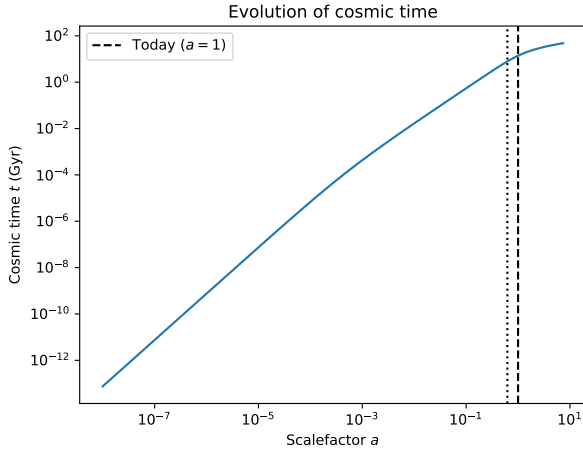

FIG. 5. Conformal time η as a function of the scalefactor a. The vertical line at $a = 1$ shows the present day.

FIG. 4. Cosmic time t as a function of the scalefactor a. The vertical dotted line at $a = 0.62$ corresponds to the the point where the universe begins to accelerate, and the vertical dashed line at $a = 1$ shows the present day.

FIG. 6. Density parameters for matter Ω_M, radiation Ω_R and dark energy Ω_Λ as functions of the scalefactor a. The vertical line at $a = 1$ shows the present day.

dominated universe.

In Fig. 6 we have the density parameters for the different constituents of the universe as functions of the scalefactor a. From the plot we can see that the beginning of the universe was radiation dominated, that is, most of the universe consisted of photons and neutrinos. As the universe expanded, the radiation density decreased, and the matter density increased. In other words, the amount of baryons and cold dark matter increased. After a while, the amount of matter also started to decrease, and the dark energy density started increasing. Today (shown as a vertical dashed line in the figure), dark energy makes up most of the universe, while the rest of the universe
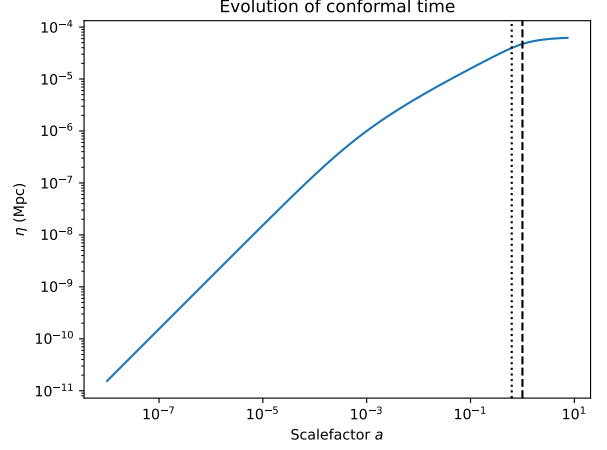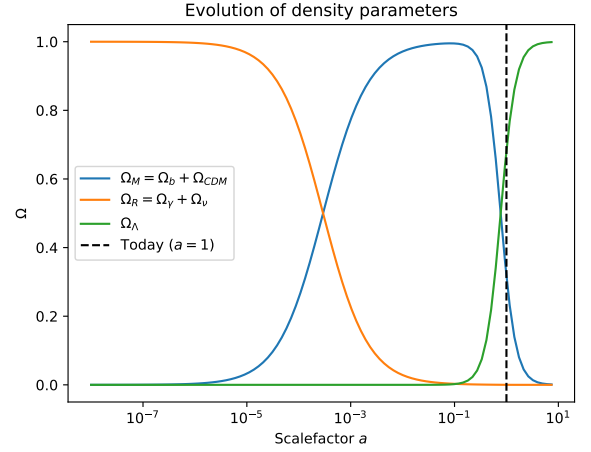
consists mainly of baryons and cold dark matter.

The luminosity distance d_L from the supernova dataset [2] is shown in Fig. 7 as a function of redshift z, together with the theoretical prediction from our code. The theoretical prediction is not a perfect fit to the dataset. It follows a similar trend, as the curve bends upward in the same manner as the datapoints, but it lies outside the errorbars of quite a few of the datapoints.

In Fig. 8 we have a scatter plot showing the value of Ω_M and Ω_Λ for each sample in the MCMC simulation. The plot shows constraints on the fraction of matter and dark energy in the universe. In other words, according to the simulation, the fraction of matter and dark energy in the universe is very unlikely to be outside the points shown in the figure. More precisely, the 1σ constraint contains 68.3% of the samples, and the 2σ constraint con-
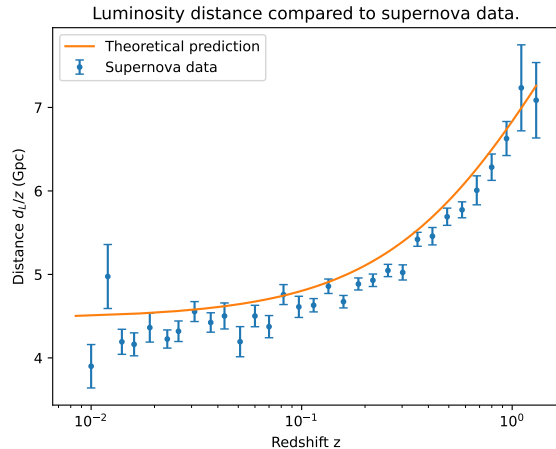
FIG. 7. Comparison of the scaled luminosity distance $\frac{d_L}{z}$ as a function of redshift z, between the supernova data and our theoretical prediction. The supernova data is retrieved from [2].

FIG. 8. Distribution of density parameters for matter Ω_M and dark energy Ω_Λ from the Markov chain Monte Carlo (MCMC) method. Each point plotted in the figure represents Ω_M and Ω_Λ for one MCMC sample. The 1σ and 2σ constraints refers to what samples we have included in the plot, namely the values corresponding to χ^2 being within one and two standard deviations respectively. The dashed line shows every value where $\Omega_M + \Omega_\Lambda = 1$, i.e., where the universe consists of only matter and dark energy, thus where the universe is flat.

tains 95.45% of the samples [5]. The scatter plot does not appear to restrict the possible matter-dark energy fraction very much. If we had included results from other observations as well, the samples from the different observations would intersect each other, and in that way restrict the possible fractions further, as shown in [2]. Although Fig. 8 does not restrict the matter-dark energy fraction too much, it does seem to imply very strongly that the dark energy density is non-zero. In other words, the observational data presented in [2] is a strong indication of the existence of dark energy, and thereby the acceleration of the universe.

In Fig. 9 we have plotted a histogram, showing the probability distribution for the Hubble parameter H_0 from the different samples in the MCMC simulation. The normal distribution plotted together with the histogram fits well with the samples, showing that the samples are normally distributed. The best fit value from the MCMC simulation is 0.70. This is way higher than the Planck best fit of 0.67 [3], which is not even shown in Fig. 9. It would be very interesting to further examine why our results deviate so greatly from [3].

In Table I we have included some specific values of time variables at four different times in the history of the universe. We see that the matter-radiation equality happened very early in the universe, after only $5.0 \cdot 10^{-5}$Gyr after the big bang, or $50\,000$ years. At this point the universe was only $3.0 \cdot 10^{-4}$ the size of today, with the observable universe reaching $\eta = 115$Mpc in radius. The redshift is very large at $z = 3.3 \cdot 10^3$, which corresponds to light at this time being highly redshifted today after traveling for so long in an expanding universe. 7.87Gyr after the big bang, the universe began to accelerate. At this point the universe was 0.62 the size it is today, and the observable universe had a radius of $\eta = 11.9$Gpc. The
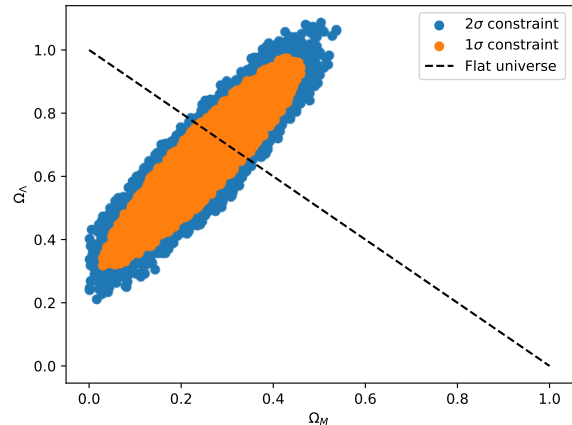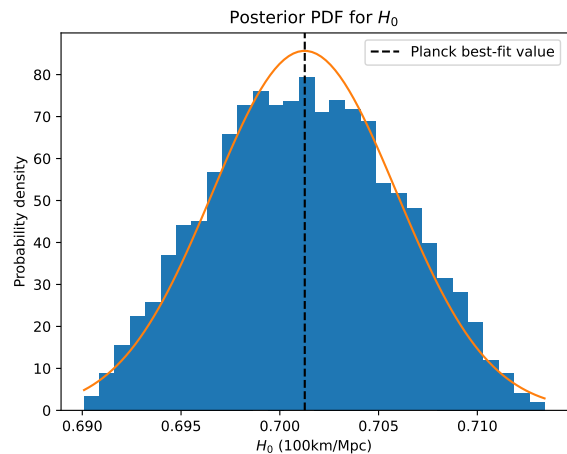

FIG. 9. Histogram showing the frequency of different values of the Hubble parameter H_0 from the Markov chain Monte Carlo (MCMC) samples. The vertical line shows the best fit value of H_0, i.e, the value corresponding to the sample with the lowest χ^2 value. The orange curve shows a normal distribution corresponding to the mean value and standard deviations of H_0 from the across the MCMC samples.

redshift at this point has also decreased largely since the matter-radiation equality epoch, at $z = 0.61$. The next epoch was when the amount of matter and the amount of dark energy were equal. This happened 10.21Gyr after the big bang, and at this point the size of the universe was 0.76 of what it is today. The observable universe was

$\eta = 12.9 \text{Gpc}$ in radius, and the redshift had dropped to $z = 0.31$.

The last row in Table I shows the time variable's values today. Since we have used discretized numerical values, they are not exact, which is why we have $a = 0.94$ instead of $a = 1$. The redshift should also be $z = 0$ today, since light emitted today will not be redshifted due to the expansion of the universe when it hits us. The time $t = 12.96 \text{Gyr}$ is our estimate of the age of the universe based on the numerical computations. This estimate is quite a bit lower than the value of 13.80Gyr obtained by [3]. This mismatch could be related to the fact that our measure of 'today' in Table I is not as exact as we would want it to be. It could also stem from insufficient accuracy in the numerical computations. We found the radius of the observable universe today to be $\eta = 13.9 \text{Gpc}$, which (up to decimal precision) coincides perfectly with the value of 14Gpc given by [6].

III. MILESTONE II
RECOMBINATION HISTORY

The early universe was very hot and dense, consisting of high-energy photons and free electrons. It was essentially opaque, since any photons proagating through space could not move very far before scattering off the free electrons and change direction. As the universe got colder, electrons were able to bind to protons, forming hydrogen atoms, without high-energy photons ripping them apart. This period in the history of the universe is known as recombination, and leads to photons being able to travel further distances without scattering off free electrons, and the universe became transparent. The recom- bination period is very important for us in understanding the CMB power spectrum, since the CMB is radiation that has traveled to us from the opaque universe just before recombination. In this milestone we look at the time when recombination happens. We compute the free electron fraction of the universe at different times, as well as the optical depth and visibility functions, and use these values to compute what times decoupling and recombination happens. We also compute the sound-horizon at decoupling, since this value will be relevant for the next parts of the project.

A. Theory

1. The Boltzmann equation

When finding the time of recombination, we want to know how many particles of different types that are present at any time. For this, we have the distribution function $f(t, \vec{x}, \vec{p})$, which gives the number of particles of a particular type. The evolution of f is given by the Boltzmann equation,

$$\frac{df}{dt} = C[f], \tag{23}$$

where $C[f]$ is the collision term, telling us how the particle interacts with other particles. Expanding the left hand side of the equation, we get

$$\frac{\partial f}{\partial t} + \frac{\partial f}{\partial x^i}\frac{dx^i}{dt} + \frac{\partial f}{\partial E}\frac{dE}{dt} + \frac{\partial f}{\partial \hat{p}^i}\frac{d\hat{p}^i}{dt} = C[f]. \tag{24}$$

The collision term we will work with is that of the process $1 + 2 \leftrightarrow 3 + 4$, for which the collision term is

$$C(f_1) = \int \frac{d^3 p_2}{(2\pi)^3 2E_2} \int \frac{d^3 p_3}{(2\pi)^3 2E_3} \int \frac{d^3 p_4}{(2\pi)^3 2E_4} \times \tag{25}$$

$$\times |\mathcal{M}|^2 (2\pi)\delta(E_1 + E_2 - E_3 - E_4)(2\pi)^3 \delta^{(3)}(\vec{p}_1 + \vec{p}_2 - \vec{p}_3 - \vec{p}_4) \times \tag{26}$$

$$\times [f_3 f_4 (1 \pm f_1)(1 \pm f_2) - f_1 f_2 (1 \pm f_3)(1 \pm f_4)], \tag{27}$$

where $\mathcal{M}$ is the matrix element of the interaction (related to the probability of the interaction happening), $\delta(x)$ and $\delta^{(3)}(x)$ are the one- and three-dimensional Dirac delta functions, and the indices $1, 2, 3$ and 4 correspond to the different particles of the interaction.

2. The Saha equation

Electrons and protons come together to form hydrogen atoms, and high-energy photons cause hydrogen atoms to split back into free electrons and protons. This interaction can be represented as

$$e^- + p^+ \rightleftharpoons H + \gamma. \tag{28}$$

The universe is electrically neutral, which gives $n_e = n_p$, where n_i is the number density of constituent i. In this report, we assume that the only atoms being formed in the universe are hydrogen atoms, i.e. we neglect helium and heavier atoms. This gives us the the number density

TABLE I. Values of different time variables at certain points in time. The first row shows when we have matter-radiation equality. The second row shows when the universe begins to accelerate (i.e, when $\frac{d\mathcal{H}}{dx} = \dot{a}$ becomes positive). The third row shows when we have matter-dark energy equality. The last row shows the value of the time variables today[a]. The rows are sorted by increasing time. The first column shows the scalefactor a. The second column shows the redshift z. The third column shows the cosmic time t, and the last column shows the conformal time η.

	a	z	t (Gyr)	η (Mpc)
$\Omega_M = \Omega_R$	$3.0 \cdot 10^{-4}$	$3.3 \cdot 10^3$	$5.0 \cdot 10^{-5}$	$1.15 \cdot 10^2$
Universe accelerates	0.62	0.61	7.87	$1.19 \cdot 10^4$
$\Omega_M = \Omega_\Lambda$	0.76	0.31	10.21	$1.29 \cdot 10^4$
Today	0.94	0.0647	12.96	$1.39 \cdot 10^4$

[a] 'Today' refers to the point in time when $a = 1$, but since we are working with discrete numerical values, we did not have a precise $a = 1$ datapoint, but have instead used the scalefactor closest to 1, which in our case was $a = 0.94$.

for baryons,

$$n_b \approx n_H = \frac{\rho_b}{m_H} = \frac{\Omega_{b0}\rho_{c0}}{m_H a^3} \qquad (29)$$

where m_H is the hydrogen mass, and $\rho_{c0} = \frac{3H_0^2}{8\pi G}$ is the critical density today. We want to find the number density of electrons, and do this by defining the free electron density $X_e = \frac{n_e}{n_b}$. The free electron density will then give us the fraction of the baryons today that are electrons, meaning X_e will be between 0 and 1. In other words, if $X_e = 1$, there are no hydrogens in the universe, and all electrons are free. If $X_e = 0$ there are no free electrons, since they are all bound to atoms.

Using Eq. 24 and Eq. 27, and assuming that the interactions are close to equilibrium, we arrive at the Saha equation

$$\frac{X_e^2}{(1 - X_e)} = \frac{1}{n_b}\left(\frac{k_b T m_e}{2\pi\hbar^2}\right)^{3/2} e^{-\frac{\epsilon_0}{k_b T}}, \qquad (30)$$

where m_e is the electron mass, k_b is the Boltzmann's constant, $\hbar$ is Planck's constant, and ϵ_0 is the electric permittivity in vacuum.

3. The Peebles equation

Eq. 30 is an approximation, and it is only valid when we are close to equilibrium. When we move away from equilibrium, we will switch to the Peebles equation given by

$$\frac{dX_e}{dx} = \frac{C_r(T_b)}{H}\left[\beta(T_b)(1 - X_e) - n_H \alpha^{(2)}(T_b) X_e^2\right]. \qquad (31)$$

The expressions for the parameters in the Peebles equation are given by

$$C_r(T_b) = \frac{\Lambda_{2s \to 1s} + \Lambda_\alpha}{\Lambda_{2s \to 1s} + \Lambda_\alpha + \beta^{(2)}(T_b)}, \qquad (32a)$$

$$\Lambda_{2s \to 1s} = 8.227 \text{s}^{-1}, \qquad (32b)$$

$$\Lambda_\alpha = H\frac{(3\epsilon_0)^3}{(8\pi)^2 c^3 \hbar^3 n_{1s}}, \qquad (32c)$$

$$n_{1s} = (1 - X_e)n_H, \qquad (32d)$$

$$n_H = n_b = \frac{3H_0^2 \Omega_{b0}}{8\pi G m_H a^3}, \qquad (32e)$$

$$\beta^{(2)}(T_b) = \beta(T_b)e^{\frac{3\epsilon_0}{4k_b T_b}}, \qquad (32f)$$

$$\beta(T_b) = \alpha^{(2)}(T_b)\left(\frac{m_e k_b T_b}{2\pi\hbar^2}\right)^{3/2} e^{-\frac{\epsilon_0}{k_b T_b}}, \qquad (32g)$$

$$\alpha^{(2)}(T_b) = \frac{8}{\sqrt{3\pi}}c\sigma_T\sqrt{\frac{\epsilon_0}{k_b T_b}}\phi_2(T_b), \qquad (32h)$$

$$\phi_2(T_b) = 0.448\ln\left(\frac{\epsilon_0}{k_b T_b}\right). \qquad (32i)$$

4. The optical depth

When light moves through a medium, some of the photons will be absorbed, reducing the overall intensity. If the light was emitted from a source with intensity I_0, then an observer at a time x will observe an intensity of

$$I(x) = I_0 e^{-\tau(x)}, \qquad (33)$$

where $\tau(x)$ is called the optical depth. The larger the optical depth is, the less one would see, so $\tau \gg 1$ means we would see nothing, and $\tau \ll 1$ means it would be as if the medium wasn't there. In our case, the medium light travels through is a universe consisting of free electrons, thus the observed intensity is low when the density of free electrons are high, and vice versa. We can find the optical depth from the differential equation

$$\frac{d\tau}{dx} = -\frac{cn_e\sigma_T}{H}, \qquad (34)$$

where $\sigma_T = \frac{8\pi}{3}\frac{\alpha^2\hbar^2}{m_e^2c^2}$ is the Thomson scattering cross section given by particle physics, and α is the fine-structure constant.

5. The visibility function

From the optical depth we can define the visibility function

$$\tilde{g}(x) = \frac{d}{dx}e^{-\tau} = -\frac{d\tau}{dx}e^{-\tau}. \qquad (35)$$

The visibility function is a probability distribution, telling us what the probability that some photon was last scattered at time x. Since $\tilde{g}$ is a probability distribution, it must be normalized, i.e., it must satisfy

$$\int_{-\infty}^{0} \tilde{g}(x)\,dx = 1. \qquad (36)$$

6. The sound-horizon

We also want to compute the sound-horizon at decoupling r_s, which is the distance a sound-wave can travel in the photon-baryon plasma from the big bang until photons decouple. The sound-horizon $s(x)$ at a time x is given by

$$\frac{ds(x)}{dx} = \frac{c_s}{\mathcal{H}}, \qquad (37)$$

where $c_s = c\sqrt{\frac{R}{3(1+R)}}$, and $R = \frac{4\Omega_{\gamma 0}}{3\Omega_{b0}a}$. Thus the sound-horizon at decoupling is given by $r_s = s(x_{\text{decoupling}})$.

B. Implementation details

We first computed the free electron fraction X_e using the Saha equation, Eq. 30, and the Peebles equation Eq. 31. First, we rewrote Eq. 30 in a way that is more familiar for quadratic equations,

$$X_e^2 + c(x)X_e - c(x) = 0, \qquad (38)$$

with

$$c(x) = \frac{1}{n_b}\left(\frac{k_bTm_e}{2\pi\hbar^2}\right)^{3/2}e^{-\frac{\epsilon_0}{k_bT}}. \qquad (39)$$

Solving the quadratic equation gives

$$X_e = \frac{-c + \sqrt{c^2 + 4c}}{2}, \qquad (40)$$

where we have neglected the minus sign, since $\sqrt{c^2 + 4c} > c$, and it does not make sense to have $X_e < 0$. For large

c, we can Taylor expand the square root in Eq. 40 to get

$$X_e = \frac{1}{2}(-c + \sqrt{c^2 + 4c})$$
$$= \frac{1}{2}\left(-c + c\sqrt{1 + \frac{4}{c}}\right)$$
$$\approx \frac{1}{2}\left(-c + c\left(1 + \frac{2}{c}\right)\right)$$
$$= \frac{1}{2}(-c + c + 2)$$
$$X_e \approx 1,$$

when c is very large. In our code we have used this approximation when $\frac{1}{c} < 10^{-4}$.

When $X_e \leq 0.99$ we switched to the Peebles equation, since the Saha equation is only valid close to equilibrium. We solved the Peebles equation using a Runge-Kutta 4 solver, just as we did in Section II.

After computing the free electron fraction X_e, we computed the optical depth τ from Eq. 34, and the visibility function $\tilde{g}$ from Eq. 35. Eq. 34 was solved using the same Runge-Kutta 4 solver as for the Peebles equation, with the initial condition $\tau(x = 0) = 0$, and then Eq. 35 was solved directly from $\tau(x)$.

We also computed the times x, z and t for decoupling and recombination, where we use $\tau = 1$ for decoupling, and $X_e = 0.1$ for recombination, and we computed the freeze-out abundance of electrons $X_e(x = 0)$.

Lastly we computed the sound-horizon at decoupling r_s by solving Eq. 37 with initial condition $s(x_{\text{ini}}) = \frac{c_s(x_{\text{ini}})}{\mathcal{H}(x_{\text{ini}})}$, again using the Runge-Kutta 4 solver.

C. Results

In Fig. 10 we have plotted the free electron fraction X_e as a function of the scalefactor a, including what it would look like if we used the Saha-approximation the whole time. We see that $X_e = 1$ at very early times. This is exactly what we would expect, since the early universe was too hot for electrons to bind to protons and form hydrogen atoms, thus all electrons in the universe were free. When the temperature drops sufficiently, recombination happens, and the electrons start binding to protons in the universe, creating stable hydrogen atoms. This can be seen in Fig. 10 by X_e beginning to drop rapidly at around $a = 9.3 \cdot 10^{-4}$ (marked by a vertical dashed line). Today the universe mostly consists of bound atom states, which is why we see X_e stabilizing close to zero after recombination, at $X_e = 2.0 \cdot 10^{-4}$. It is more apparent in Fig. 11 that the free electron fraction is not exactly zero. This figure is identical to Fig. 10, except with a logarithmic y-axis. Here we also see that the Saha approximation keeps decreasing rapidly, and it actually reaches zero.

There are several reasons why the free electron fraction today is not actually zero. Although the number of
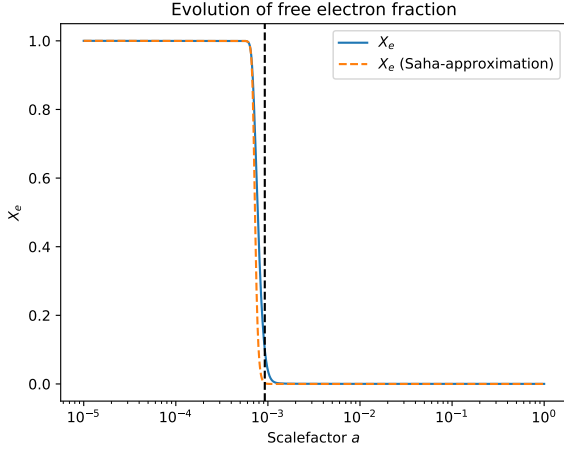
FIG. 10. The free electron fraction X_e as a function of the scalefactor a. The dashed orange curve represents X_e according to the Saha approximation, and the vertical dashed line shows the scalefactor at recombination.

FIG. 12. The optical depth τ, and its first and second derivatives $\frac{d\tau}{dx}$ and $\frac{d^2\tau}{dx^2}$, as functions of the scalefactor a. The vertical dashed line shows the scalefactor at recombination.
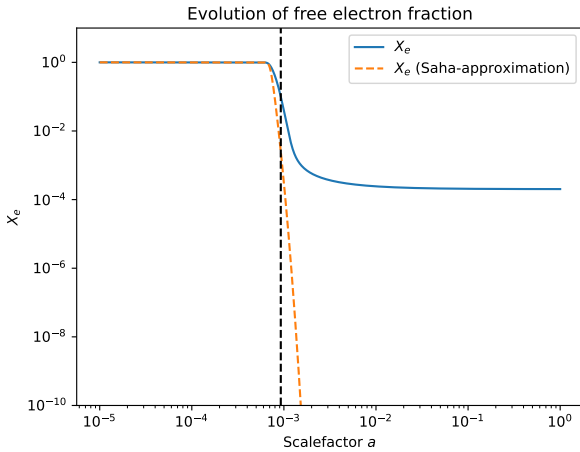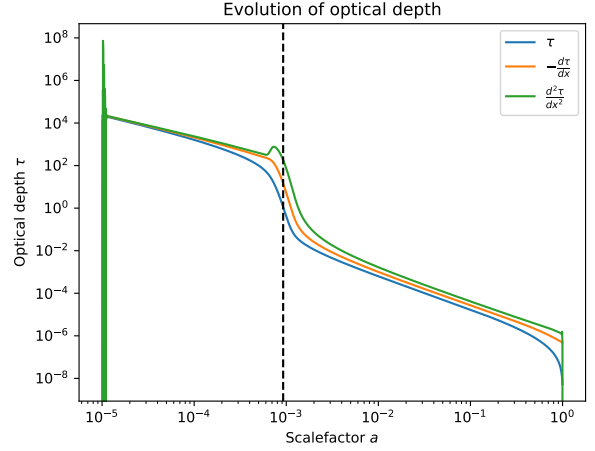

FIG. 11. The same plot as in Fig. 10, but here with a logarithmic y-axis to better show the difference between the predicted free electron fraction, and how it would look according to the Saha approximation.

protons and electrons in the universe overall are the same (the universe is electrically neutral), some parts of space will contain more or less protons than electrons. As the universe expands, the particles spread further, and these uneven distributions of electrons and protons increase. In the parts of space where the distribution is uneven, there will be leftover electrons or protons after recombination that are too far apart to form hydrogen atoms. In addition, even though the average temperature of the photons has decreased, there will still be some high-energy photons left. These high-energy photons can still rip atoms apart into protons and electrons.

In Fig. 12 we can see the evolution of the optical depth τ and it's first and second derivatives. We can see that τ

starts out very large, meaning we would not be able to see anything in the very early universe due to photons scattering off free electrons. τ then slowly decreases until it reaches recombination, represented by a vertical dashed line, where it drops rapidly. This is because the free electrons in the universe starts forming bound hydrogen atoms at this point, which means photons can start moving more freely. After recombination, the optical depth starts decreasing slowly again, and continues in that way until today. The slow decrease in the optical depth before and after recombination comes from the expansion of the universe. As the universe expands, the free electrons become less dense, giving photons more room to move. The effect of the expansion of the universe is however not as significant as when the number of free electrons decreases during recombination, which is why the slope is much less steep before and after recombination than during.

In Fig. 13 we see the visibility function $\tilde{g}$ as a function of x, as well as its first and second derivatives. In the early universe, $\tilde{g} = 0$, which corresponds well with our description of a dense universe with photons scattering off free electrons before being able to move anywhere. At recombination the free electrons bind to protons, forming hydrogen atoms, giving photons room to move. Therefore, the photons we observe today have a high probability of coming from recombination, which is why $\tilde{g}$ peaks at recombination, represented by a vertical dashed line in Fig. 13. After recombination, $\tilde{g}$ again goes to zero. This is because the probability of photons we observe today to have last scattered at a time much later than recombination is very low, since there are hardly any free electrons to scatter off of. We often refer to recombination as the surface of last scattering, and this comes from the fact that $\tilde{g}$, which is a probability distribution for when photons we observe last scattered, peaks at recombination.
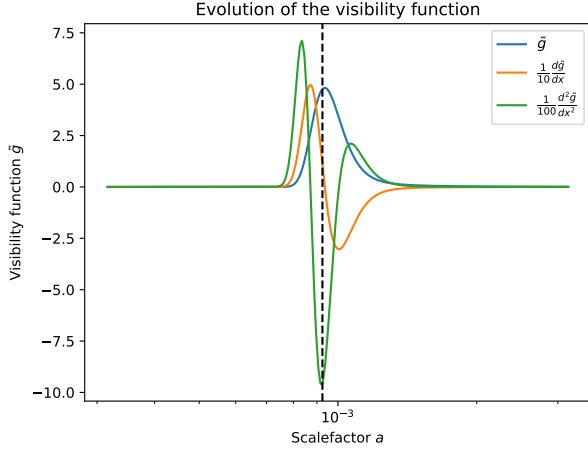
FIG. 13. The visibility function $\tilde{g}$ and its first and second derivatives $\frac{d\tilde{g}}{dx}$ and $\frac{d^2\tilde{g}}{dx^2}$, as functions of the scalefactor a. The derivatives have been scaled to fit in the same figure as $\tilde{g}$. The vertical dashed line shows the scalefactor at recombination.

In Table II we show the computed times for when decoupling and recombination happens. We see that we get a redshift at recombination of $z = 1.08 \cdot 10^3$, which compared to the value of $z = 1090$ given in the Planck paper[3] gives a relative error of only 0.9%. After recombination, decoupling happens very quickly, only $60\,000$ years later. This makes sense, as the two are closely related. When the free electrons bind to protons and form hydrogen, the photons decouple as they can start moving more freely.

Lastly, we also computed the sound-horizon $r_s =$ 146Mpc. This value is also close to the Planck paper[3], which found $r_s = 144$Mpc, thus giving a relative error of only 1.4%. Our results seem to coincide well with the Planck paper[3] considering that we ignore the formation of helium and heavier elements.

IV. MILESTONE III
EVOLUTION OF STRUCTURE IN THE UNIVERSE

INTRODUCTION

A. Theory

B. Implementation details

C. Results

V. MILESTONE IV
THE CMB AND MATTER POWER-SPECTRA

INTRODUCTION

A. Theory

B. Implementation details

C. Results

VI. CONCLUSION

Conclusion

[1] H. A. Winther, H. K. Eriksen, Ø. Elgarøy, D. F. Mota, and H. Ihle, Cosmology II a course on the formation of the cosmic microwave background and structures in the universe (2021-2024).

[2] M. Betoule, R. Kessler, J. Guy, J. Mosher, D. Hardin, R. Biswas, P. Astier, P. El-Hage, M. Konig, S. Kuhlmann, J. Marriner, R. Pain, N. Regnault, C. Balland, B. A. Bassett, P. J. Brown, H. Campbell, R. G. Carlberg, F. Cellier-Holzem, D. Cinabro, A. Conley, C. B. D'Andrea, D. L. DePoy, M. Doi, R. S. Ellis, S. Fabbro, A. V. Filippenko, R. J. Foley, J. A. Frieman, D. Fouchez, L. Galbany, A. Goobar, R. R. Gupta, G. J. Hill, R. Hlozek, C. J. Hogan, I. M. Hook, D. A. Howell, S. W. Jha, L. Le Guillou, G. Leloudas, C. Lidman, J. L. Marshall, A. Möller, A. M. Mourão, J. Neveu, R. Nichol, M. D. Olmstead, N. Palanque-Delabrouille, S. Perlmutter, J. L. Prieto, C. J. Pritchet, M. Richmond, A. G. Riess, V. Ruhlmann-Kleider, M. Sako, K. Schahmaneche, D. P. Schneider, M. Smith, J. Sollerman, M. Sullivan, N. A. Walton, and C. J. Wheeler, Astronomy & Astrophysics **568**, A22 (2014).

[3] N. Aghanim, Y. Akrami, M. Ashdown, J. Aumont, C. Baccigalupi, M. Ballardini, A. J. Banday, R. B. Barreiro, N. Bartolo, S. Basak, R. Battye, K. Benabed, J.-P. Bernard, M. Bersanelli, P. Bielewicz, J. J. Bock, J. R. Bond, J. Borrill, F. R. Bouchet, F. Boulanger, M. Bucher, C. Burigana, R. C. Butler, E. Calabrese, J.-F. Cardoso, J. Carron, A. Challinor, H. C. Chiang, J. Chluba, L. P. L. Colombo, C. Combet, D. Contreras, B. P. Crill, F. Cuttaia, P. de Bernardis, G. de Zotti, J. Delabrouille, J.-M. Delouis, E. Di Valentino, J. M. Diego, O. Doré, M. Douspis, A. Ducout, X. Dupac, S. Dusini, G. Efstathiou, F. Elsner, T. A. Enßlin, H. K. Eriksen, Y. Fantaye, M. Farhang, J. Fergusson, R. Fernandez-Cobos, F. Finelli, F. Forastieri, M. Frailis, A. A. Fraisse, E. Franceschi, A. Frolov, S. Galeotta, S. Galli, K. Ganga, R. T. Génova-Santos, M. Gerbino, T. Ghosh, J. González-Nuevo, K. M. Górski, S. Gratton, A. Gruppuso, J. E. Gudmundsson, J. Hamann, W. Handley, F. K. Hansen, D. Herranz, S. R. Hildebrandt, E. Hivon, Z. Huang, A. H. Jaffe, W. C. Jones, A. Karakci, E. Keihänen, R. Keskitalo, K. Kiiveri, J. Kim, T. S. Kisner, L. Knox, N. Krachmalnicoff, M. Kunz, H. Kurki-Suonio, G. Lagache, J.-M. Lamarre, A. Lasenby, M. Lat-

TABLE II. Values of scalefactor a, redshift z and cosmic time t at recombination and decoupling.

	a	z	t (Gyr)
Recombination ($X_e = 0.1$)	$9.25 \cdot 10^{-4}$	$1.08 \cdot 10^3$	$3.78 \cdot 10^{-4}$
Decoupling ($\tau = 1$)	$9.34 \cdot 10^{-4}$	$1.07 \cdot 10^3$	$3.84 \cdot 10^{-4}$

tanzi, C. R. Lawrence, M. Le Jeune, P. Lemos, J. Lesgourgues, F. Levrier, A. Lewis, M. Liguori, P. B. Lilje, M. Lilley, V. Lindholm, M. López-Caniego, P. M. Lubin, Y.-Z. Ma, J. F. Macías-Pérez, G. Maggio, D. Maino, N. Mandolesi, A. Mangilli, A. Marcos-Caballero, M. Maris, P. G. Martin, M. Martinelli, E. Martínez-González, S. Matarrese, N. Mauri, J. D. McEwen, P. R. Meinhold, A. Melchiorri, A. Mennella, M. Migliaccio, M. Millea, S. Mitra, M.-A. Miville-Deschênes, D. Molinari, L. Montier, G. Morgante, A. Moss, P. Natoli, H. U. Nørgaard-Nielsen, L. Pagano, D. Paoletti, B. Partridge, G. Patanchon, H. V. Peiris, F. Perrotta, V. Pettorino, F. Piacentini, L. Polastri, G. Polenta, J.-L. Puget, J. P. Rachen, M. Reinecke, M. Remazeilles, A. Renzi, G. Rocha, C. Rosset, G. Roudier, J. A. Rubiño-Martín, B. Ruiz-Granados, L. Salvati, M. Sandri, M. Savelainen, D. Scott, E. P. S. Shellard, C. Sirignano, G. Sirri, L. D. Spencer, R. Sunyaev, A.-S. Suur-Uski, J. A. Tauber, D. Tavagnacco, M. Tenti, L. Toffolatti, M. Tomasi, T. Trombetti, L. Valenziano, J. Valiviita, B. Van Tent, L. Vibert, P. Vielva, F. Villa, N. Vittorio, B. D. Wandelt, I. K. Wehus, M. White, S. D. M. White, A. Zacchei, and A. Zonca, Astronomy & Astrophysics **641**, A6 (2020).

[4] N. Metropolis, A. W. Rosenbluth, M. N. Rosenbluth, A. H. Teller, and E. Teller, The Journal of Chemical Physics **21**, 1087 (1953), https://pubs.aip.org/aip/jcp/article-pdf/21/6/1087/18802390/1087_1_online.pdf.

[5] R. Reid, Chi-squared distribution table with sigma values, https://www.reid.ai/2012/09/chi-squared-distribution-table-with.html (2012).

[6] J. R. Gott III, M. Jurić, D. Schlegel, F. Hoyle, M. Vogeley, M. Tegmark, N. Bahcall, and J. Brinkmann, The Astrophysical Journal **624**, 463–484 (2005).

[7] P. Callin, How to calculate the cmb spectrum (2006), arXiv:astro-ph/0606683 [astro-ph].